First-principles studies of the $\Sigma 5$ tilt grain boundary in Ni_3Al

Gang Lu, Nicholas Kioussis, and R. Wu
Department of Physics, California State University Northridge, Northridge, California 91330-8268

Mikael Ciftan
Physics Division, U.S. Army Research Office, Research Triangle Park, North Carolina 27709-2211

(Received 14 May 1998)

The atomic and the electronic structures of the $\Sigma 5$ (210) [001] tilt grain boundary in Ni_3Al, with and without a hydrogen impurity, have been calculated using the full potential linearized-augmented plane-wave method. The strain field normal to the boundary plane and the excess grain boundary volume are calculated and compared with the results obtained using the embedded-atom method (EAM). The interlayer strain normal to the grain boundary oscillates with increasing distance from the grain boundary. The bonding charge distributions suggest that bonding in the boundary region is different from that in the bulk. Total-energy calculations show that the hydrogen impurity prefers to occupy interstitial sites on the Ni-rich grain boundary plane. Hydrogen is found to reduce the bonding charge across the boundary plane. The grain boundary energy and the Griffith cohesive energy for both the ''clean'' and H-segregated grain boundary are calculated and compared with the available EAM results. The hydrogen impurity is found to increase the grain boundary energy and reduce the Griffith cohesive energy of the boundary, which indicates that hydrogen is an embrittler of the grain boundary. [S0163-1829(98)04245-3]

I. INTRODUCTION

It is by now well established that grain boundaries play important roles in metallic alloys affecting their mechanical, electrical, and even chemical properties.[1,2] There are strong indications that grain boundaries in intermetallic compounds behave uniquely and thus present some very interesting properties which are technologically and scientifically important. More specifically, the $L1_2$-type ordered Ni_3Al alloys exhibit unique thermomechanical properties that make them attractive for structural applications at elevated temperatures.[3] Among these are their high melting temperature, low density, resistance to corrosion, and most importantly their high specific strength that *increases* with temperature. However, polycrystalline ordered stoichiometric Ni_3Al alloys have an inherent drawback, namely, their tendency for brittle intergranular fracture,[3] even though single crystals of these alloys are highly ductile. This propensity towards intergranular fracture is traced to the reduced cohesion between adjacent grains at their shared grain boundaries, particularly to the structural and atomic compositional details at these grain boundaries, including various impurities that diffuse and segregate in these domains from the bulk.[4]

The main purpose of the present work is to apply *ab initio* electronic structure calculations to investigate the electronic origin which is responsible for such characteristic grain boundary properties. In the present paper we investigate the grain boundary properties of the $\Sigma 5$ (210) [001] tilt grain boundary in the ordered Ni_3Al alloy, for both the ''clean'' stoichiometric case as well as the case with a hydrogen impurity placed in various interstitial sites. The purpose of this work is to gain insight on how the local environment at the grain boundary changes the bonding charge distribution from that in the bulk, and how this bonding charge in turn changes in the presence of the impurity. The calculations are self-consistent microscopic quantum-mechanical calculations, which include structural relaxations, with specificity down to the electronic-chemical hybridized bonding and antibonding orbitals of the host and impurity atoms at the grain boundary. Pictorial representations of the resulting *bonding* charge distributions offer an intuitive insight as to why and how cracks might propagate along the grain boundary.

It has been observed that different types of grain boundaries in the same material seem to have different resistance to fracture.[5] Some, such as the $\Sigma 3$ type grain boundary, are more resistant to cracking and some are weaker. However, it is not simply the type of structure alone that determines the propensity towards fracture. It is also known that specific impurity atoms in the alloy, such as sulfur and boron play opposite roles on grain boundary cohesion; sulfur reduces the ductility of the alloy by decreasing the fracture resistance,[6] while boron sharply increases the ductility and completely supresses brittle intergranular fracture.[4] Based on such experimental evidence, attempts are being made to engineer the grain boundary by microalloying or macroalloying with such impurities.[4] The present study is an attempt, in part, to determine to what extent the theoretical tools in hand are capable of contributing to this thrust. Since hydrogen is a prime example of an element that segregates to the grain boundary and causes intergranular embrittlement in the Ni_3Al alloy,[7] we shall study its effect on the grain boundary cohesion in detail in this paper.

While significant experimental and theoretical progress have been made in understanding grain boundaries in pure systems,[8–10] the level of understanding of the role that grain boundaries play in alloy systems is much less developed. Atomistic simulations utilizing pair potentials or the embedded-atom method (EAM) (Refs. 11–16) have been used with great success to study the atomic structure of grain

boundaries in metals and in intermetallics. However, these methods involving the process of fitting parameters, are limited in determining accurate energetics for grain boundaries, and fail to provide insight into the chemical bonding characteristics from which ensue to cohesiveness of interatomic forces which control grain boundary properties. In contrast to empirical methods such as the EAM, first-principles electronic structure calculations based on the density-functional theory are applicable to a much broader range of elements and bonding environments; thus they allow the possibility of not only studying ''clean'' grain boundaries, but also grain boundaries containing chemically different impurities. Using cluster electronic structure calculations, Eberhart and Vvedensky[17] suggested that the appearance of localized grain boundary electronic states above the Fermi energy in Ni_3Al, with considerably less directional charge distribution than that found in the parent crystal, provides an indication of intergranular fracture. The present study differs from these previous cluster calculations in that the present ones are fully relaxed self-consistent full-potential total-energy calculations with no shape approximations to the potential and charge density. It must be noted that electronic structure calculations using small ($\approx$10 atoms) clusters while revealing gross trends, do suffer from the uncontrolled effects of free boundaries.[17–19] In the present work we shall be taking a large enough set of atoms to minimize this problem and we will show below *a posteriori*—see the oscillatory behavior achieved after relaxation in Fig. 2—that the surface effects are minimized in our calculations. Thus, we can provide valuable information about the structural relaxations responsible for the grain boundary volume expansion, and about the redistribution of bonding charge across and parallel to the boundary plane.

Grain boundaries in intermetallic alloys behave uniquely and thus present some very interesting properties.[20] In perfect lattices of intermetallic compounds, i.e., mostly ordered alloys, such as the $L1_2$-type ordered nickel-based Ni_3X *(X* =Al, Ga, Si, Ge, Mn) compounds, atoms of one component (Ni) prefer to bind with atoms of the other component atom *(X)* as their nearest neighbors owing to their chemical bonding nature. In these ordered alloys the binding of Ni-*X* bond is much stronger than the average binding energies of Ni-Ni and *X*-*X* bonds. However, within the grain boundary region of these alloys the ordered structure is partially destroyed and thus this rule may not hold. Thus, grain boundaries in intermetallics may involve *bond defects* in addition to the lattice distortions.[21] Indeed we shall show that these *bond defects* give rise to a redistribution of *bonding* charge, which could potentially modify the crack propagation characteristics along the boundary in Ni_3Al.

Beyond these rearrangements of atomic constituents of the pure compound and beyond the role of specific impurities that may segregate into the grain boundary causing further bonding rearrangements, there is also the important issue of stoichiometry that may affect the grain boundary structure. The stoichiometry has been found to have a very strong effect on the grain boundary strength; grain boundaries that contain excess Ni atoms seem to be more resistant to fracture.[22] We shall also see below that our calculations do substantiate this observation.

All in all, we shall see that the electronic structure and the nature of the chemical bonds can influence the cohesion of the grains at their shared grain boundaries with distinct directionality—tensorial character—and these in turn become related to the mechanical properties of the intermetallic alloys, such as their propensity to intergranular fracture. These then may suggest ways of introducing appropriate impurities into an engineered or microstructured grain boundary to achieve a particular mechanical behavior, if at all possible.

In Sec. II, we briefly describe the full-potential linearized-augmented plane wave (FLAPW) method and discuss the slab model used in the grain boundary electronic structure calculations. In Sec. III, we describe the numerical results of the electronic structure for the clean $\Sigma5$ Ni_3Al grain boundary. We present results for the displacements of the atomic planes away from the grain boundary which show a decaying oscillatory relaxation superimposed on a net expansion which is similar to that seen in the vicinity of free surfaces. The results for the changes of the electronic structure induced by the hydrogen impurity are presented in Sec. IV A, and those for the energetics are discussed in Sec. IV B. Finally, in Sec. V a brief summary and statement of conclusions are presented.

II. MODEL AND COMPUTATION

The electronic structure of the grain boundary is calculated by means of *ab initio* total-energy electronic structure calculations based on the full-potential linearized-augmented plane wave method[23] with the atomic force approach.[24] In the FLAPW method, no shape approximation is being made for the charge, potential, and wave functions. Within the muffin-tin spheres ($s_{MT,Ni}=s_{MT,Al}=2.0$ a.u.), lattice harmonics with angular-momentum 1 up to 8 are adopted. Energy cutoffs of 13 and 100 Ry are employed for the plane wave basis and star functions to describe the wave functions, charge density, and potential in the interstitial region, respectively. Convergence is assumed when the root-mean-square difference between the input and output charge density becomes less than $1\times10^{-4}e/(\text{a.u.})^3$. The step-forward fixed basis approach[10] is used to speed up the calculations. The interplanar distances of *all* layers in the slab are adjusted efficiently according to the calculated forces. The equilibrium atomic geometry is assumed when the atomic forces on each atom normal to the grain boundary is less than 0.05 eV/Å.

The grain boundary of $\Sigma5$ [001](210) is constructed by means of the coincidence site lattice (CSL) model. The grain boundary is simulated by a slab model with eleven (210) layers as shown in Fig. 1(a). The slab model is chosen to minimize the grain boundary interactions inherent to a superlattice cell model. With five layers in between, the interaction between the free surface (introduced artificially in the slab model) and the grain boundary is expected to be sufficiently reduced. The two-dimensional lattice constant is set equal to the experimental value of $a=3.56$ Å for bulk Ni_3Al.[5] All layers have been relaxed according to the forces except the surface layers fixed at their bulk positions in order to eliminate the free surface effects. The unrelaxed slab geometry for the $\Sigma5$ (210) tilt grain boundary of Ni_3Al viewed along the [001] direction are shown in Fig. 1(a). The cell

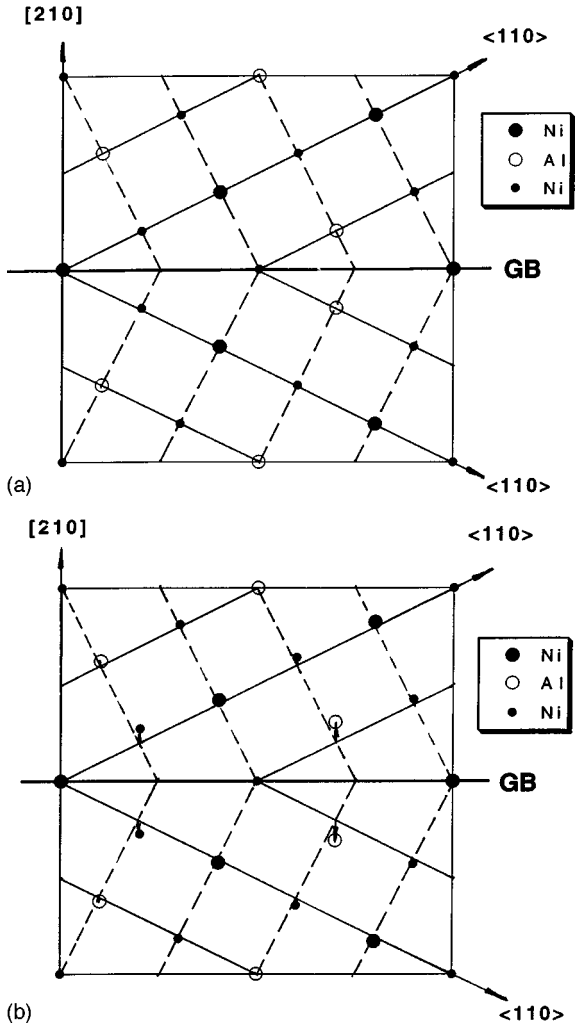

FIG. 1. Unrelaxed (a) and relaxed (b) slab geometry for the $\Sigma=5$ (210) [001] tilt grain boundary in Ni_3Al viewed along the $\langle 001 \rangle$ direction. The large and small circles represent atoms on two (001) atomic planes, respectively, and the open and closed circles correspond to Al atoms and Ni atoms, respectively.

consists of two (001) planes and eleven (210) layers. The large and small circles represent atoms distributed on the first (001) atomic plane and the second (001) atomic plane, respectively, and open and closed circles correspond to Al atoms and Ni atoms, respectively. Note that in the grain boundary region of the $L1_2$ intermetallic compounds, wrong bonds between like atoms [Ni-Ni and Al-Al in Fig. 1(a)] are introduced across the grain boundary and thus proper bonds with unlike atoms are not conserved.

III. CLEAN GRAIN BOUNDARY

A. Atomic structure

The relaxed grain boundary atomic structure is shown in Fig. 1(b) and the arrows show the relaxation vectors. The calculated displacements normal to the grain boundary for the three (210) layers nearest to the boundary plane are listed in Table I. These displacements are obtained by subtracting the unrelaxed atomic positions normal to the boundary plane from the relaxed atomic positions. The Ni(1) and Ni(2) atoms on the second (210) layer are located on two different

TABLE I. Calculated values of the atomic displacements (in a.u.) normal to the grain boundary, for the three (210) layers which are nearest to the Σ5 (210) Ni_3Al grain boundary plane.

Layer	Atom	Normal displacement (a.u.)
1	Ni	0.58
1	Al	0.82
2	Ni(1)	0.19
2	Ni(2)	0.13
3	Al	0.32
3	Ni	0.17

(001) planes. One can see that the largest displacement occurs at the first layer parallel to the grain boundary. We shall see in more detail in Sec. III B below, that the larger relative displacement of the nearest-neighbor Al atoms across the grain boundary compared to that of the Ni atoms, is due to the depletion of bonding charge at the Al site which leads to a stronger electrostatic repulsion between the Al-Al atoms. This in turn gives rise to the rippling effect close to the boundary interface similar to that observed in the clean Ni_3Al (100) surface.[25]

It is a well known result that the interlayer spacing near a relaxed free surface show an oscillatory pattern which decays into the bulk when far away from the surface.[25] It is interesting to notice that similar atomic relaxation occurs also in the vicinity of the grain boundary.[26] Figure 2 shows the normal strain component (ϵ_{zz}) as a function of the layer away from the boundary plane. One can see a symmetric oscillatory strain profile that has a maximum at the boundary plane and decays into the bulk. The strain oscillations of the grain boundary in Ni_3Al are similar to those found near the symmetric tilt boundaries in aluminum.[14] The nature of this strain profile can be traced to the dislocation interaction at low angle boundaries,[27] but it seems to be valid also at high angle boundaries, such as this case of 36.87°. The small strain of the fourth layer indicates that the effect of strain is localized only within several layers from the boundary plane. Therefore the 11 layers slab used in these calculations is large enough to capture the overall properties of the grain boundary.

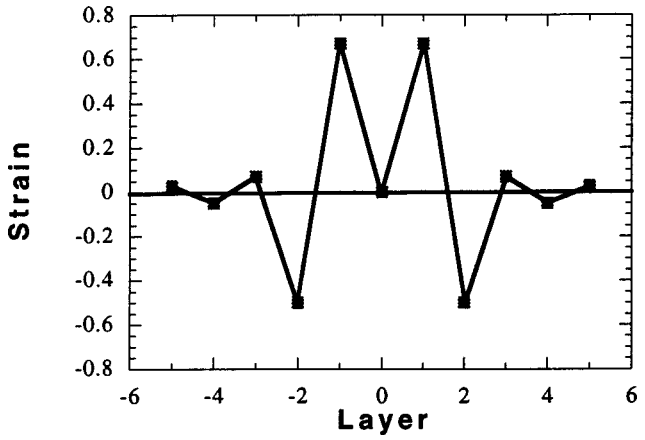

FIG. 2. The relative deviation of interlayer spacing normal to the grain boundary plane ϵ_{zz} as a function of the number of layers away from the (210) tilt grain boundary.

One local measure for the grain boundary expansion is the relative normal displacement of the two atomic planes closest to the boundary plane. This local measure of excess grain boundary volume can be calculated from the average displacements of the Ni and Al atoms.[14] The present electronic structure calculations yield a local expansion of 0.63 a.u. (or $0.1a_0$, where a_0 is the bulk Ni_3Al lattice constant). Embedded atom calculations for the pure Ni and Al $\Sigma 5$ (210) grain boundaries give similar values for the local expansion of $0.1a_{Ni}$ and $0.13a_{Al}$, respectively.[14]

B. Bonding charge density distribution

In order to gain insight at the microscopic level of the change of bonding at the grain boundary from that in the bulk, we have calculated the *bonding* charge density for both the bulk Ni_3Al system and the grain boundary. The bonding charge density is defined as the difference between the total charge density in the solid and the superpositions of neutral atomic charge densities placed at lattice sites.[28] The bonding charge density represents the net charge redistribution as atoms are brought together to form the crystal or the grain boundary. The relative redistribution of the bonding normal to and parallel to the boundary interface is responsible for the cohesion and the mechanical properties of the boundary.

The bonding charge density for the bulk system on the (001) and (002) planes is shown in Figs. 3(a) and 3(b), respectively. The (001) plane contains both Al and Ni atoms, while the (002) plane contains solely Ni atoms as in the grain boundary. The solid (dotted) contours represent accumulation (depletion) of electronic charge. The bonding charge on the (001) plane is mainly due to the Al/p-Ni/d hybridization and that on the (002) plane is due to Ni/d-Ni/d hybridization. It can be seen that the bonding between the nearest-neighbor (NN) Al and Ni atoms on the (001) plane is mostly ionic in nature; charge is transferred from Al to Ni, which is in accord with the Pauling electronegativity difference. On the (002) plane, the d-d hybridization between the NN Ni atoms results in a charge difference which shows a dd-π bonding character.

As in the case of bulk, we can see in Fig. 4(a) that in the grain boundary the depletion of electron density at the Al sites is accompanied by significant *anisotropic* build-up of the directional d-bonding charge at the Ni sites. The bonding directionality is mainly caused by the polarization of p electrons at the Al sites as a result of the bonding charge density on the (001) plane [Fig. 4(a)] in the grain boundary which has changed greatly from that in the bulk. In general, the bonding charge across the grain boundary is greatly reduced. On the other hand, bonding parallel to the interface develops along the Ni-Ni line between the NN Al pairs across the boundary, which contributes very little, if any, to the grain boundary cohesion. This ''spilled-out'' charge accumulation is within a very thin range and extends only to about 0.2 Å away from the boundary plane. The bonding further away is more bulklike, namely, the bonding charge accumulation at the Ni site is along the nearest-neighbor Ni-Al and the next-nearest-neighbor Ni-Ni directions.

The bonding charge on the (002) plane in Fig. 4(b) shows a similar large charge depletion along the grain boundary over an area which is more than half of the entire interface

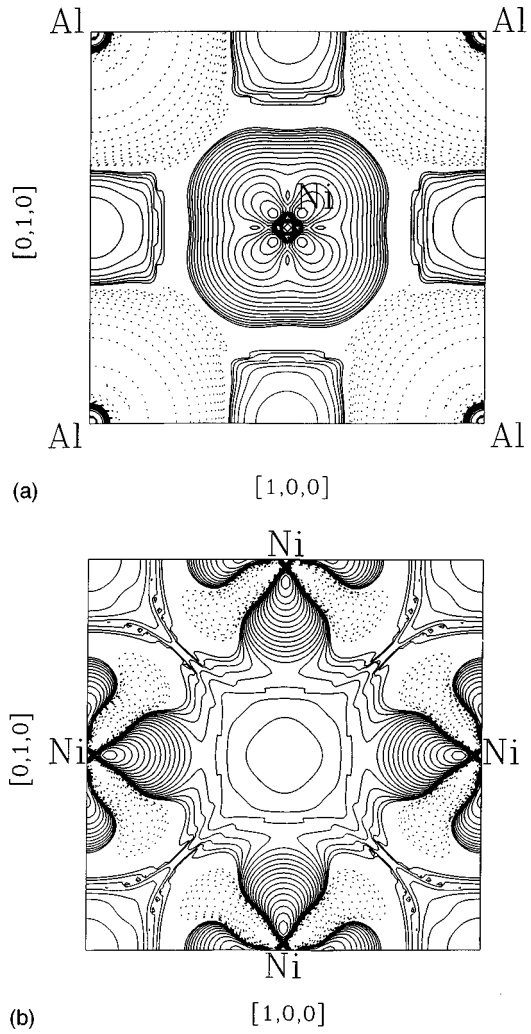

FIG. 3. Bonding charge density of bulk Ni_3Al, (a) on the (001) Ni-Al mixed plane and (b) the (002) pure Ni plane. Solid (dotted) contours represent contours of increased (decreased) charge density. Contours start from $\pm 4.0\times 10^{-4} e/(\text{a.u.})^3$ and increase successively by a factor of root 2.

area. It is interesting to note that while away from the interface the bonding charge is along the next-nearest-neighbor Ni-Ni direction [refer to the square in Fig. 4(b)], the bonding direction of the Ni atom on the boundary plane has changed to parallel to the interface. The accumulation of isotropic (s-like) interstitial bonding charge between the nearest-neighbor Ni-Ni atoms on the (002) plane across the boundary plane, increases the bonding normal to the grain boundary; this indicates the importance of the Ni atoms in holding the grain boundary together. Thus, replacement of the two nearest-neighbor Al atoms across the grain boundary by Ni atoms would lead to an increased cohesion between the two grains. This is consistent with the experimental results that the Ni-rich boundary is more resistant to intergranular fracture.[6,29] If a boron impurity is introduced to the grain boundary region, it will occupy the regions of charge depletion and bridge the bonding between Ni atoms on the (002) plane across the interface and increase the grain boundary cohesion. The opposite effect of H impurity will be discussed later in the paper. It should be emphasized that this type of information cannot be supplied by empirical techniques such as the EAM.

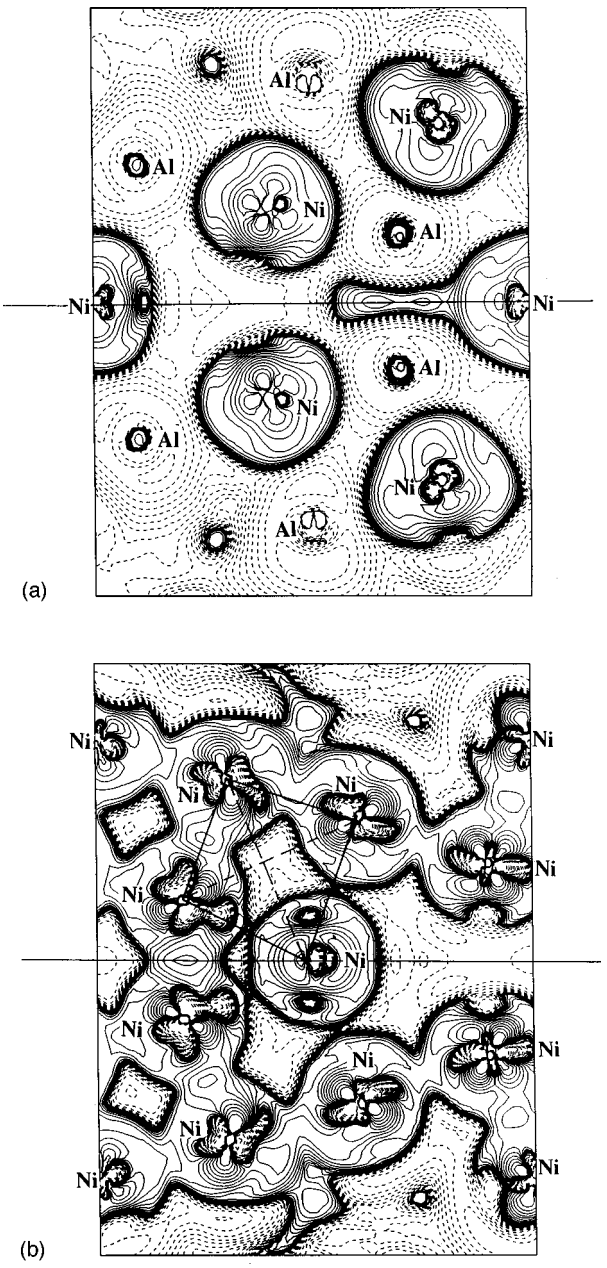

FIG. 4. Bonding charge density of the Σ5 grain boundary, (a) on the (001) Ni-Al mixed plane and (b) on the (002) pure Ni plane, respectively. Solid (dotted) contours represent contours of increased (decreased) charge density. Contours start from $\pm 4.0\times 10^{-4} e/(\text{a.u.})^3$ and increase successively by a factor of root 2.

C. Density of states

In Figs. 5(a) and 5(b) we show the total density of states (DOS) for the bulk and the Σ5 grain boundary in Ni_3Al, respectively. The density of states of the grain boundary are obtained from the atoms within only two layers from the boundary plane, thus excluding the contributions from the surface introduced artificially in the slab. A characteristic feature of the DOS of the bulk Ni_3X (X=Al, Si, Ga) systems, is the hybridization between the X p and Ni d states.[30] As shown in Fig. 5(a) a sharp bonding (antibonding) peak is located in the region near −3.4 eV (1.3 eV) in bulk Ni_3Al. Another feature of the electronic structure in the bulk case is

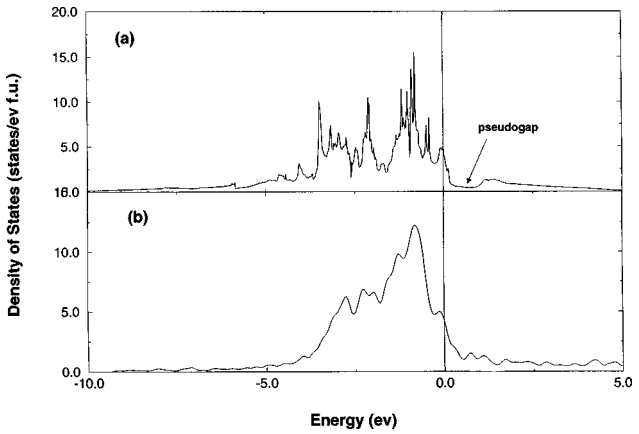

FIG. 5. Total density of states for (a) the bulk Ni_3Al lattice and (b) the Σ5 grain boundary.

a valley (pseudogap) located about 0.5 eV above the Fermi energy, which separates the p-d bonding and antibonding states. In Ni_3Al, the Ni-d hole states above the Fermi energy are antibonding states of t_{2g}-t_{2g} σ type. As we can see from Fig. 5(b), the pseudogap in the DOS disappears in the case of the grain boundary. Rather than forming a gap, certain localized states appear above the Fermi energy. These states arise from hybridization of the Ni d-p and Al s states.

D. Grain boundary energetics

The grain boundary energy can be determined from the difference of the energy of a unit slab cell containing the grain boundary and the energy of a slab cell containing an equal number of each type of atoms in the bulk environment, divided by the total grain boundary area. In order to eliminate the surface effect induced by the slab model, we choose another slab to model the bulk environment. This slab has the same surfaces as in the grain boundary case and contains the same number of Ni and Al atoms. Our calculation for the grain boundary energy should be reliable because it removes the energy contribution from the surface by employing a slab cell for both the grain boundary and the bulk. The slab model for the grain boundary eliminates the grain boundary interactions inherent in a superlattice cell model. For the Σ5 boundary, we find a grain boundary energy of 1.7 J/m^2 for the 22-atom unit cell, which is larger than the 1.2–1.4 J/m^2 given by the EAM.[14] This result seems to support the argument that the grain boundary and stacking fault energy given by density functional theory are larger than that from the EAM although the EAM calculation provide a good description of the structural properties.[9]

The Griffith cohesive energy is defined as the energy required to cleave a brittle material without plastic deformation. When the material is cleaved along a grain boundary, two free surfaces are created and the grain boundary is destroyed. The grain boundary cohesive energy (Griffith energy) is

$$\gamma_{\text{coh}} = \gamma_{s1} + \gamma_{s2} - \gamma_{\text{gb}}, \tag{1}$$

where γ_{s1} and γ_{s2} are the two surface energies, which are different due to the different atomic composition and γ_{gb} is the grain boundary energy. Cleavage of the Σ5 (210) [001]

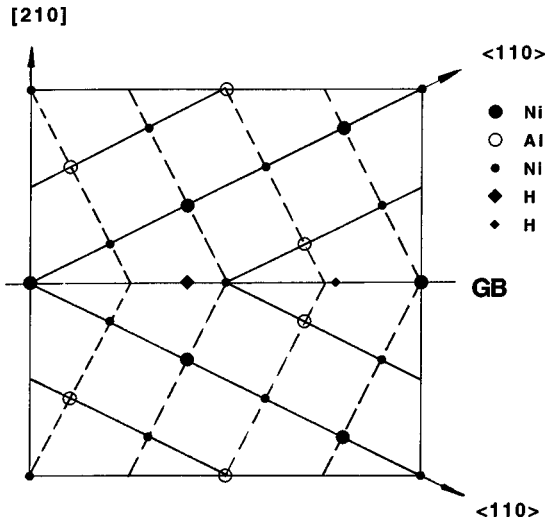

FIG. 6. Unrelaxed slab geometry for the $\Sigma=5$ (210) [001] tilt grain boundary in Ni_3Al viewed along the $\langle 001 \rangle$ direction. The large and small diamonds represent the hydrogen impurity on the mixed (001) Ni-Al and the pure (002) Ni plane, respectively.

grain boundary results in a mixed Ni-Al (210) surface containing 50% Ni and 50% Al, and a pure Ni (210) surface containing 100% Ni. We find that the energies of the relaxed mixed Ni-Al and pure Ni surfaces are 2.03 and 2.17 J/m^2, respectively, and that the Griffith cohesive energy is 2.5 J/m^2 compared to the value of 3.8 J/m^2 obtained from EAM calculations.[14] This result is reasonable, since the grain boundary energies and the cohesive energies are, crudely, inversely related.

IV. EFFECT OF HYDROGEN ON GRAIN BOUNDARY

It is well known that hydrogen segregates to grain boundaries and occupies interstitial sites, owing to its exceptional mobility in the lattice at low temperatures, strong attraction to voids, ability to capture vacancies and ability to migrate with dislocations.[31] Hydrogen is known to reduce the grain boundary cohesion. In this section we present *ab initio* total-energy electronic structure calculations to understand the role that hydrogen plays in the cohesion of the $\Sigma5$ grain boundary in Ni_3Al.

In order to study the effect of the local environment of the hydrogen impurity on the electronic structure, the impurity was placed at two different interstitial sites: (1) on the Ni-Al mixed (001) plane and (2) the pure Ni (002) plane, as shown in Fig. 6. The large and small diamonds represent the hydrogen impurity in the (001) and the (002) plane, respectively. The total energy of the relaxed configuration for the latter case is lower by 0.03 eV compared to the first, indicating that hydrogen prefers to segregate to the Ni-rich (002) boundary plane. Previous calculations[28] for bulk Ni_3Al, have shown that hydrogen prefers to occupy Ni-rich octahedral sites. The difference in energy for H at the two different sites is mainly due to the H-Al interaction which is only present in one case. We found that Al-H interaction leads to some charge transfer between H and Al, which results in lowered band energy but increased electrostatic energy. The net result is the increased total energy for H at the Ni-deficient sites.

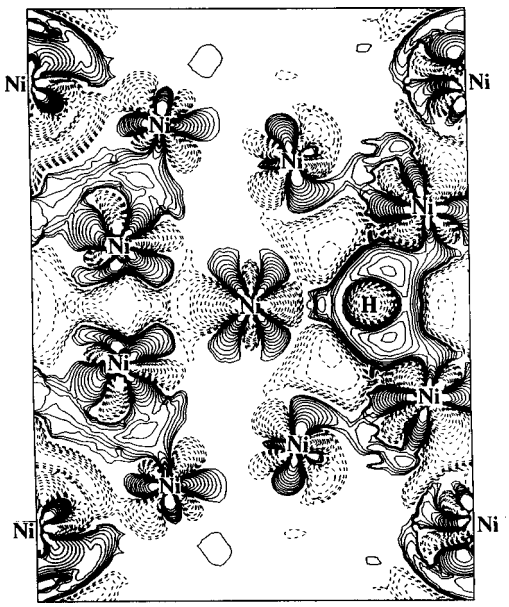

FIG. 7. Hydrogen-induced charge density of the $\Sigma5$ grain boundary in Ni_3Al on the (002) plane. Hydrogen occupies the interstitial site (labeled by the small diamond in Fig. 6) on the pure Ni (002) plane. Solid (dotted) contours represent contours of increased (decreased) charge density. Contours start from $\pm 4.0\times10^{-4} e/(\text{a.u.})^3$ and increase successively by a factor of root 2.

A. Hydrogen-induced bonding charge

To understand the effect of hydrogen on the bonding charge properties of the grain boundary we consider the redistribution of bonding charge induced by the impurity atom when placed at the interstitial site. This can be best described by the *difference of bonding charge density* between the pure and H-doped grain boundaries, namely,

$$\Delta\rho_{\text{ind}}(r) = \Delta\rho_{\text{solid}}(\text{Ni}_3\text{AlH}) - \Delta\rho_{\text{solid}}(\text{Ni}_3\text{Al}) = \rho_{\text{solid}}(\text{Ni}_3\text{AlH}) - \rho_{\text{solid}}(\text{Ni}_3\text{Al}) - \rho_{\text{atom}}(\text{H}). \quad (2)$$

We will refer to $\Delta\rho_{\text{ind}}(r)$ as the *hydrogen-induced bonding* charge density.[28] The H-induced bonding charge density on the (002) plane (pure Ni plane) is shown in Fig. 7. Here, solid and dotted curves represent contours of increased (accumulation) and decreased (depletion) bonding charge density. Comparison of Figs. 3(b) and 7 shows that H induces a significant redistribution of bonding charge of the Ni atom at the interface. The hybridization between the hydrogen and the Ni atom at the grain boundary, of the $3d_{z^2}$-$1s\sigma$ type, results in a reduction of the bonding charge parallel to the boundary compared to the pure grain boundary; and a charge buildup in the t_{2g}-type antibonding d orbitals pointing along the Ni-Ni direction (d_{xz}). This charge redistribution results in an enhancement of the bonding-charge directionality of the Ni atom at the grain boundary. More importantly, the more or less isotropic bonding charge between the nearest-neighbor Ni atoms across the grain boundary has been greatly reduced, and these two atoms develop bonding somewhat parallel to the interface. Keeping in mind that the bonding normal to the boundary plane between the two Ni atoms is the most important contribution to the cohesive force

which holds the two grains together, this bonding picture reveals the electronic origin for the H-induced intergranular brittleness in polycrystalline Ni_3Al. Overall, a comparison of Figs. 4(b) and 7 does suggest that hydrogen decreases the local grain boundary cohesion. This is certainly consistent with its role as an embrittling element.

B. Grain boundary energetics

A thermodynamic theory developed by Rice and co-workers[32] describes the mechanism of metalloid-induced intergranular embrittlement through competition between crack blunting versus brittle separation. The theory predicts that the potency of a segregating impurity in reducing the ''Griffith work'' of brittle boundary separation is a linear function of the difference $\Delta E_b - \Delta E_s$, i.e., the difference between the segregation energy for that solute at a grain boundary and at a free surface. Thus, an impurity with more positive energy difference will be a more potent embrittler, or vice versa. Using the present state-of-the-art electronic structure calculations, we can explore the embrittlement problem from the point of view of the total energy differences between the grain boundary and the free surface systems. For the H-Ni_3Al free surface system, the Ni_3Al substrate is simulated by 11-layer slab and the hydrogen adsorbate is placed pseudomorphically on similar interstitial sites on both sides of the slab. The impurity-induced structural relaxations were included in all calculations.

We have calculated the hydrogen formation energies at the grain boundary $\Delta E_{gb} = E_{gb}(\mathrm{GB+H}) - E_{gb}(\mathrm{GB})$, and at the free surface $\Delta E_s = E_s(S+\mathrm{H}) - E_s(S)$, respectively. The calculated hydrogen formation energies at the grain boundary is -15.31 eV, whereas that at the free surface is -16.12 eV. Thus, $\Delta E_{gb} - \Delta E_s = 1.4\ \mathrm{eV} > 0$, indicates that hydrogen is an embrittling element, in agreement with experimental results.

We have calculated also the grain boundary energy in the presence of H impurity. In this case, the grain boundary energy is calculated from the difference in the total energy of the grain boundary with the H impurity placed interstitially [pure Ni (002) plane] and the total energy of the bulk with the H impurity placed at a similar interstitial site. For the bulk calculation, the H is placed at an octahedral Ni-rich site. The grain boundary energy in the presence of the hydrogen impurity is found to be 2.14 J/m^2. Comparison with the results in Sec. III D indicates that the impurity has increased the grain boundary energy and hence this grain boundary is not as stable as the parent ''clean'' grain boundary. Unfortunately, we are not aware of any theoretical or experimental result on the grain boundary with hydrogen in order to make a comparison.

V. CONCLUSION

We have studied the atomic and electronic structures of the Σ5 (210) [001] grain boundary in Ni_3Al with and without H impurity employing first principles electronic structure calculations based on the full-potential linearized augmented plane wave (FLAPW) method with the atomic force approach.

For the ''clean'' grain boundary we find that the relaxed interlayer strain perpendicular to the grain boundary shows an oscillatory behavior with a rapidly decaying profile with increasing distance from the boundary plane. The excess grain boundary volume is 0.1 a_0 and the grain boundary relaxation energy is about 0.8 eV/slab. The bonding charge distribution in the boundary region is different from that in the bulk due to the different atomic rearrangement (''bond defects''). In general, the bonding charge across the grain boundary is reduced in both the (001) and (002) planes. The directionality of the bonding charge of the Ni atom at the grain boundary has changed and is parallel to the interface. The accumulation of bonding interstitial charge across the nearest-neighbor Ni pair on the (002) plane increases the bonding normal to the interface. The disappearance of the pseudogap in the density of states on going from the bulk Ni_3Al system to the grain boundary, is indicative of a reduced mechanical stability of the interface relative to the parent crystal. The grain boundary energy and the Griffith cohesive energy of the pure grain boundary have been calculated and compared with the results of the EAM calculations.

Hydrogen prefers to occupy interstitial sites on the Ni-rich (002) boundary planes. Hydrogen is found to reduce in general the bonding between the Ni atoms across the grain boundary and to enhance the bonding-charge directionality of the Ni atoms at the grain boundary. This suggests that hydrogen reduces the local grain boundary cohesion. We have employed Rice's thermodynamic model to examine the energetics of the H-induced weakening of the grain boundary cohesion. The positive difference in formation energy for hydrogen at the grain boundary ΔE_{gb} and at the free surface ΔE_s of 1.4 eV indicates the embrittling potency of hydrogen in the Ni_3Al grain boundary. Overall, we find that our calculations are in agreement with the known behavior of hydrogen in Ni_3Al, and they provide insight into the bonding behavior underlying the weakening of the grain boundary cohesion.

ACKNOWLEDGMENTS

The research was supported through the U.S. Army under Grant No. DAAG55-97-1-0093, the Keck Foundation, and the Office of Research and Sponsored Projects at California State University, Northridge.

[1] *Materials Interfaces–Atomic-level Structure and Properties*, edited by D. Wolf and S. Yip (Chapman and Hall, London, 1992).

[2] *Interfaces in Crystalline Materials*, edited by A. P. Sutton and R. W. Balluffi (Oxford University Press, Oxford, 1995).

[3] *High Temperature Ordered Intermetallic Alloys*, edited by N. S. Stoloff, C. C. Koch, C. T. Liu, and O. Izumi, MRS Symposia Proceedings No. 81 (Materials Research Society, Pittsburgh, 1987).

[4] C. T. Liu and D. P. Pope, in *Intermetallic Compounds—Principles and Practices*, edited by J. H. Westbrook and R. L. Fleischer (Wiley, New York, 1995), Vol. 2, p. 17.

[5] H. Lin and D. Pope, in *High Temperature Ordered Intermetallic*

Alloys IV, edited by L. Johnson, D. P. Pope, and J. O. Stiegler, MRS Symposia Proceedings No. 213 (Materials Research Society, Pittsburgh, 1991), p. 393.
[6] K. Aoki and O. Izumi, J. Jpn. Inst. Met. **43**, 1190 (1979).
[7] E. P. George, C. T. Liu, and D. P. Pope, Scr. Metall. Mater. **27**, 365 (1992).
[8] M. C. Payne, P. D. Bristowe, and J. D. Joannopoulos, Phys. Rev. Lett. **58**, 1348 (1987); D. P. DiVincenzo, *ibid*. **56**, 1925 (1986).
[9] A. F. Wright and S. R. Atlas, Phys. Rev. B **50**, 15 248 (1994).
[10] R. Wu, A. J. Freeman, and G. B. Olson, Science **265**, 376 (1994).
[11] S. P. Chen, A. F. Voter, and D. J. Srolovitz, Scr. Metall. **20**, 1389 (1986).
[12] S. P. Chen, A. F. Voter, and D. J. Srolovitz, in *High Temperature Ordered Intermetallic Alloys* (Ref. 3), p. 45.
[13] S. P. Chen, D. J. Srolovitz, and A. F. Voter, J. Mater. Res. **4**, 62 (1989).
[14] S. P. Chen, A. F. Voter, R. C. Albers, A. M. Boring, and P. J. Hay, J. Mater. Res. **5**, 955 (1990).
[15] S. M. Foiles, in *High Temperature Ordered Intermetallic Alloys* (Ref. 3), p. 51.
[16] G. J. Ackland and V. Vitek, in *High Temperature Ordered Intermetallic Alloys III*, edited by C. T. Liu *et al.*, MRS Symposia Proceedings No. 133 (Materials Research Society, Pittsburgh, 1989), p. 105.
[17] M. E. Eberhart and D. D. Vvedensky, Phys. Rev. Lett. **58**, 61 (1986).
[18] G. S. Painter and F. Averill, Phys. Rev. Lett. **58**, 234 (1987).
[19] O. Ito and H. Tamaki, Acta Metall. Mater. **43**, 2731 (1995).
[20] T. Takasugi, *Intermetallic Compounds—Principles and Practices*, edited by J. H. Westbrook and R. L. Fleischer (Wiley, New York, 1995), Vol. 1, p. 585.
[21] T. Takasugi and O. Izumi, Acta Metall. **31**, 1187 (1983).
[22] T. Takasugi, N. Masahashi, and O. Izumi, Acta Metall. **35**, 381 (1987).
[23] E. Wimmer, H. Krakauer, M. Weinert, and A. J. Freeman, Phys. Rev. B **18**, 864 (1981), and references therein.
[24] J. M. Soler and A. R. Williams, Phys. Rev. B **40**, 1560 (1989); R. Yu, D. Singh, and H. Krakauer, *ibid*. **43**, 6411 (1992).
[25] S. P. Chen, A. F. Voter, and D. J. Srolovitz, Phys. Rev. Lett. **57**, 1308 (1986).
[26] R. Kikuchi and J. W. Cahn, Phys. Rev. B **36**, 418 (1987).
[27] J. P. Hirth and J. Lothe, *Theory of Dislocations* (McGraw-Hill, New York, 1968), p. 672.
[28] S. Sun, N. Kioussis, S. Lim, A. Gonis, and W. Gourdin, Phys. Rev. B **52**, 14 421 (1995).
[29] C. T. Liu, C. L. White, and J. A. Horton, Acta Metall. **33**, 213 (1985).
[30] D. Iotova, N. Kioussis, and S. P. Lim, Phys. Rev. B **54**, 14 413 (1996).
[31] A. H. Cottrell, Mater. Sci. Technol. **6**, 121 (1990).
[32] J. R. Rice and J. S. Wang, Mater. Sci. Eng., A **107**, 23 (1989).